Engineering persistent antimicrobial pseudo-capsids

Ibolya E Kepiro,[1] Irene Marzuoli,[1,2] Katharine Hammond,[1, 3, 4] Xiaoliang Ba,[5] Helen Lewis,[1] Michael Shaw,[1] Smita B Gunnoo,[1] Emiliana De Santis,[1] Urszula Lapinska,[6] Stefano Pagliara,[6] Mark Holmes,[5] Christian D Lorenz,[7] Bart W Hoogenboom,[3] Franca Fraternali[2] and Maxim G Ryadnov[1,]*

[1]National Physical Laboratory, Hampton Road, Teddington, TW11 0LW, UK

[2]Randall Centre for Cell and Molecular Biophysics, King's College London, London, SE1 1UL, UK

[3]Department of Physics and Astronomy, University College London, London, WC1E 6BT, UK

[4]London Centre for Nanotechnology, University College London, London, WC1H 0AH, UK

[5]Department of Veterinary Medicine, University of Cambridge, Cambridge, CB3 0ES, UK

[6]Living Systems Institute, University of Exeter, Exeter, EX4 4QD, UK

[7]Department of Physics, King's College London, Strand Lane, London WC2R 2LS, UK

Corresponding author:

Dr Maxim G Ryadnov

National Physical Laboratory,

Hampton Road, Teddington, TW11 0LW, UK

Fax: (+44) 20 86140573

Tel: (+44) 20 89436078

max.ryadnov@npl.co.uk

ABSTRACT: the spread of bacterial strains persistent to antibiotic treatments stimulates the search for an alternative means of antimicrobial interventions. Here we report a virus-like pseudo-capsid engineered to self-assemble from re-purposed effector domains of a host defence protein to exhibit a broad spectrum of antibacterial activities in vitro and in vivo. Using a combination of nanoscale and single-cell imaging we demonstrate that such pseudo-capsids inflict instantaneous and all-out damage to bacterial cells by penetrating and disrupting their membranes. Unlike conventional antibiotics, these agents are effective against phenotypic bacterial variants, while clearing superbugs in vivo without toxicity. The monomeric subunits of the designed pseudo-capsids can be in either epimeric form, L or D, providing a versatile platform for engineering structurally diverse and functionally persistent antimicrobial capsids.

Antimicrobial resistance is a natural process that helps bacteria adapt to new environments (*1*). The process is relentless and represents a major health threat given our dependence on antimicrobial treatments (*2*). With conventional antibiotics losing their effectivity at an alarming rate, alternative antimicrobial interventions attract an ever-increasing interest (*3*). Most compounds that are prescribed to patients today act by binding to individual intracellular targets in bacterial cells. A single genetic event is sufficient for bacteria to acquire potent counter measures. The time these take to manifest can fall within just a few years after a given antibiotic is introduced to the market (*3*). As a consequence, bacteria can develop into "superbugs" – strains that no longer respond to antibiotic treatments. The spread of these pathogens necessitates the development of novel antimicrobials that can rapidly attack a bacterial cell as a whole. This strategy may provide agents capable of killing growing, persister and dormant cells – this feat is inaccessible to conventional antibiotics (*4*). New agents should be able to differentiate between host and bacterial cells as the attack is likely to involve cell membranes. Strictly speaking, the innate immune systems of multicellular organisms do not use antibiotics. Instead, they deploy host-defence effector molecules to the sites of infection. These molecules are stand-alone

peptides or relatively small domains in globular proteins that recognise pathogen associated molecular patterns on the surfaces of microbial cells (*5*). These effector molecules are diverse in structure and origin, but share common physicochemical properties. Most of them are cationic and fold into amphipathic conformations upon binding to anionic microbial membranes (*6*). In membranes, these conformations assemble into higher-order oligomers that overcome a threshold of peptide concentration, beyond which antimicrobial effects become apparent. Reaching this concentration appears to be a limiting step in the ability of the oligomers to permeate membranes (*7*), and is more characteristic of host defence peptides, e.g. human defensins and cathelicidins (*8*), than of effector domains of multifunctional proteins, e.g. lactoferrins, that recognise pathogen surfaces without the need to self-oligomerize (*9*). Nonetheless, in free, isolated forms, these domains can oligomerize to induce bacteriostatic effects (*10*). This presents a considerable opportunity for antimicrobial engineering. Multiple copies of an isolated effector domain can be arranged to fold into a discrete and autonomous assembly. The domain copies of the assembly are ready to be deployed at the site of contact with microbial membranes, where they instantaneously deliver concentrations that significantly exceed those necessary to rupture microbial membranes. An ultimate benefit of this design is rapid and all-out damage to a microbial cell without the need for the transition from unstructured peptide monomers to membrane-active oligomers – a strategy that may be less subject to acquired resistance. However, the success of this approach relies on the ability of the effector molecules to pre-concentrate in a distinct nanoscale structure that can bind to microbial membranes.

More specifically, most bacterial cells do not exceed 0.2 to 1 μm in width. Therefore, a discrete assembly of effector domains ranging from tens to hundreds of nanometres in diameter would be sufficient to inflict irreparable damage to a bacterial cell. To be discrete at these size ranges the assembly is best confined to a platonic, symmetrical structure. The nature of the symmetry is of less importance as long as the assembly is locked into a three-dimensional form that can bind to microbial membranes. In this regard, viral capsids inspire a straightforward solution. These are self-assembled

nanoscale shells that can be commensalistic to multicellular hosts. Viruses do not kill bacteria on contact, but can provide suitable architectural templates for the capsid-like assembly of effector molecules. Resulting assemblies need not be strictly monodisperse because their designed function allows for a level of structural polymorphism that is typical of aberrant and pseudo-capsids (*11-13*). Furthermore, the assigned function imposes no *a priori* constraints on the chirality of the effector domains. Polypeptide chains of reversed chirality or all-D peptides are much more stable to proteolysis, fold in a similar manner to that of all-L peptides and are likely to be non-immunogenic (*14-17*). Antimicrobial D epimers are as effective as their L counterparts, which is consistent with that host defence peptides act by binding to the lipid components of bacterial membranes rather than dock to a specific protein (*17, 18*). Herein we demonstrate the application of the outlined principles for the design of antimicrobial pseudo-capsids or Ψ-capsids.

RESULTS

Pseudo-capsid design

Our approach adapts a short host defence motif from a multifunctional protein lactoferrin – a major component of the innate immune system (*9, 10*). The antimicrobial properties of this protein are attributed to its N-terminal domain. The domain has a broad spectrum of targets including porins, DNA, intracellular metabolites, and can stimulate the immune system by neutralising endotoxin (*19-21*). The host defence motif of the domain is a hexapeptide RRWQWR, which has strong propensity for antiparallel β-sheet conformations (*22*).

To render this motif self-complementary, the C-terminal arginine of the peptide was replaced with a glutamate. This modification facilitates inter-strand Coulombic interactions with the N-terminal arginine of the opposite β-strand. The core of the motif is also homologous to a characteristic motif of tryptophan zippers, WTW, which folds with cross-strand tryptophan rings packed tightly against one another (*23*). To capitalise on this analogy, the glutamine in the peptide was replaced with a threonyl residue. This modification supports the formation of a tryptophanyl interface to cement a β-sheet

bilayer with two cationic exteriors. In viruses, capsid proteins interface orthogonally with each other to network into penta- and hexagonal assembly units. Each of these units adopts a three-fold rotational symmetry which ensures their propagation into a closed symmetry, shell (*24*). To emulate the three-fold symmetry of native shell-like subunits, the resulting motif RRWTWE was converted into a triskel conjugate (Figs 1A and S1 in Supporting Information), with both L- and D-forms of this conjugate chemically synthesised (Fig S2).

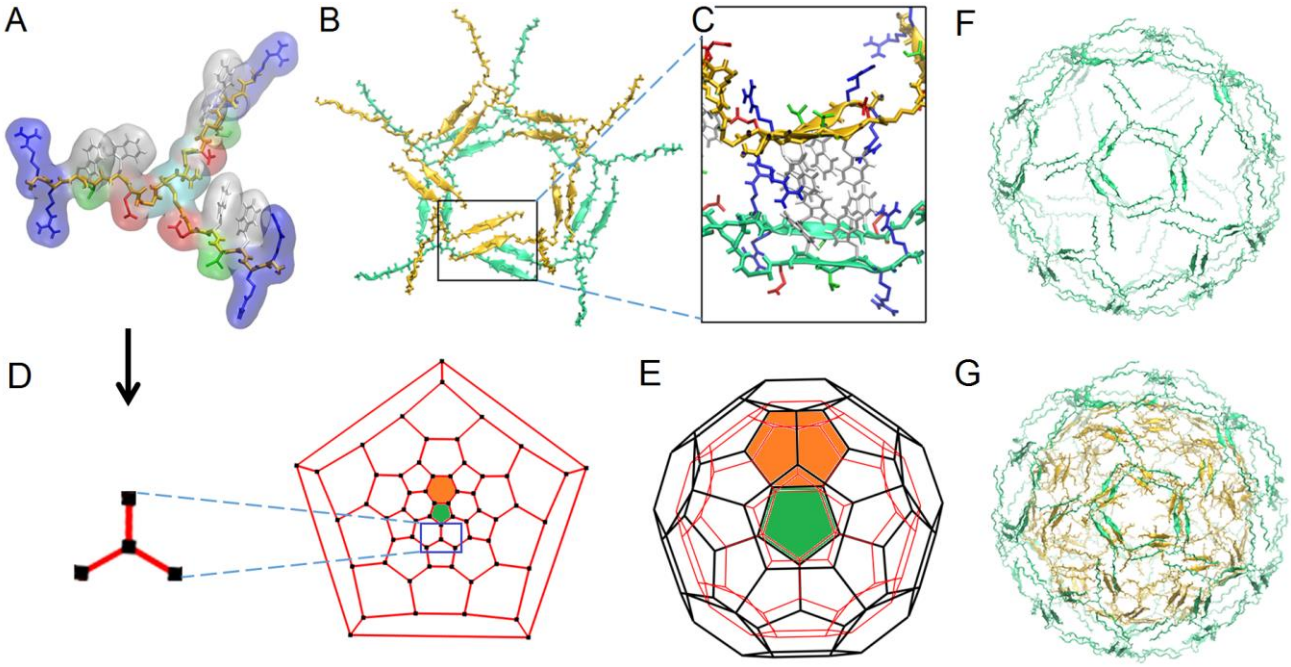

Figure 1. Pseudo-capsid design. (A) A molecular model of the triskel RRWTWE conjugate. (B) A snapshot of molecular dynamics simulations showing a pentagonal assembly unit formed by designed triskelions. (C) Two β-sheet arms (green and yellow) forming a bilayer interface via cross-strand packed tryptophans (grey). (D) A schematic representation of the designed triskelion as a monomer subunit in a truncated icosahedron shown as a 5-fold Schlegel orthographic projection. (E) 5-fold symmetry orthographic projections of two truncated icosahedra (black and red) forming a double-walled assembly. Note: for clarity only one of each of the pentagonal (green) and hexagonal (orange) units is highlighted in D and E. (F) A single-walled triskelion assembly templated on a truncated icosahedron. (G) A double-walled triskelion assembly templated on a truncated icosahedron. Outer and inner shells in (F) and (G) are shown in green and yellow, respectively.

Each arm of this triskelion pairs into an antiparallel β-sheet with another arm of another triskelion. Each folded pair of two arms interfaces with another folded pair of two other conjugates (Fig 1B, C). The monomer has a tri-lateral symmetry which enables it to assemble into penta- and hexagonal units forming β-sheet bilayer networks (Fig 1B). Because β-strands are stabilised by *inter*-strand interactions it is physically impossible for the bilayers to have free, "sticky" edges. These have to close on one another. Triskelion structures have an intrinsic non-zero curvature (*25-27*). In propagating β-sheet networks, the curvature translates into a trans-sheet asymmetry prompting the spontaneous closure of increasingly curved sheets into a minimum energy structure – shell (*27, 28*). This mode of assembly is analogous to that of viral shells which follows an icosahedral symmetry, with a truncated icosahedron being one of the most common architectures (*29, 30*). This polygon architecture offers an ideal template for the assembly of triskelions: it has only three-fold vertices, each of which can host an individual triskelion (Fig 1D, E). Therefore, the cooperative assembly of triskelions within the template should create an equilibrated β-sheet shell. The monolayer configuration of this structure is not stable as the hydrophobic side chains of the tryptophanyl residues are oriented inwards towards the water-filled core of the shell (Fig 1F). A β-sheet bilayer or a double-wall shell, in which cationic arginyl residues furnish its exterior and interior surfaces, is deemed more stable (Fig 1C, G) (*31*). In support of this conjecture, coarse grain molecular dynamics (MD) simulations (*32*) showed that single-wall icosahedra assembled from the triskelion collapsed within the first 600 ns of simulations following an equilibration phase (Fig S3A). Under the same simulation conditions, double-walled shells retained their initial configuration over 1 μs of coarse grain simulations, evolving into more compact shapes, for both L- and D-forms, which was also confirmed by 100 ns atomistic simulations (*33*) (Figs S3B, S4 and Movie S1). The results of the simulations indicate that triskelions can assemble cooperatively in the template reaching an equilibrated and stable structure.

Pseudo-capsid folding and assembly

Consistent with the simulations, Circular Dichroism (CD) spectra for both forms of the triskelion were characteristic of antiparallel β-sheet and β-turn conformations (Fig S5A). Fourier transform infrared (FT-IR) spectra revealed bands for the de-convoluted amide regions at 1650-1670 cm^{-1} for β-turn structures and at 1630 cm^{-1} and 1545 cm^{-1} for β-sheets (Fig S5B).

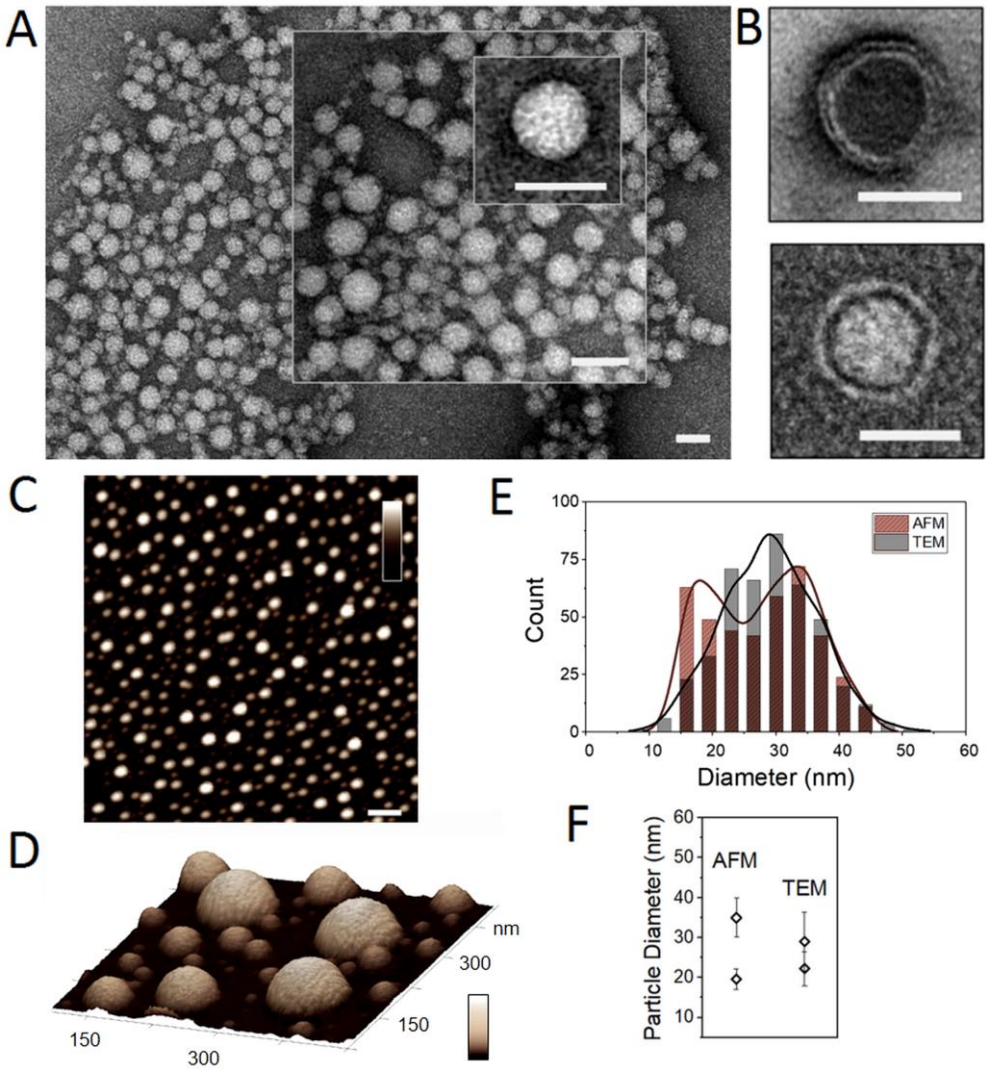

Figure 2. Pseudo-capsid assembly. (A) TEM images of assembled D-Ψ-capsids. Scale bars are 50 nm. (B) Higher resolution TEM images of individual collapsed capsids. Scale bars are 50 nm. (C) Topography images of D-Ψ-capsids obtained on a mica substrate by in liquid AFM. Colour (height) and scale bars are 60 nm and 200 nm, respectively. (D) 3D representation of D-Ψ-capsids. Colour (height) bar is 65 nm. (E) Size distributions and dominating sizes of D-Ψ-capsids by AFM and TEM. (F) Average sizes of dominating populations of Ψ-capsids. Assembly conditions: 100 μM peptide, pH 7.4, 10 mM MOPS, 20˚C, overnight.

The results suggest that inter- and intra-molecular hydrogen bonds in β-sheets and β-turns, respectively, support the cooperative folding of the triskelions into higher-order structures. Indeed, transmission electron microscopy (TEM) and atomic force microscopy (AFM), performed in solution, revealed uniformly spherical capsid-like shells (Fig 2A-D), some of which appeared to collapse into a double-walled or double-layered morphology (Fig 2B). The diameters of the shells were consistent by width (TEM) and height (AFM) measurements showing narrow step-size distributions, e.g. 10-20 nm, 20-40 nm (Fig 2E, F). This suggests that the triskelions may adopt an integer step size in assembly, generating shells that are polymorphic in size, but not in shape. This property is akin to that of viral capsids and synthetic virus-like assemblies that can adapt to repack into smaller and larger shells (*34-36*). This is also in marked contrast to mutant viral capsids and polymorphic virus-like particles whose variations in morphology feature filamentous and aberrant structures with irregular serrations (*12, 13*). Taken together the findings indicate that the designed triskelions propagate with the formation of thermodynamically stable Ψ-capsids exhibiting a degree of structural plasticity that helps accommodate size variations without compromising on morphological uniformity. Since the triskelions occupy the vertices of pentagonal and hexagonal faces in the truncated icosahedron, rather than tightly pack in the faces, the overall architecture of Ψ-capsids remains independent of size allowing for wide size variations. This property renders the assembly adaptable to morphological changes imposed by hierarchically complex and dynamic environments such as microbial membranes. To test their behaviour in membranes in sufficient detail, Ψ-capsids were introduced into reconstituted phospholipid bilayers that were assembled on mica substrates as described elsewhere (*37*). The resulting supported lipid bilayers (SLBs) provide suitable models for bacterial membranes, are flat (to within ~0.1 nm) in their unperturbed state (Fig 3A, B), and allow for the accurate depth measurements of surface changes in solution and in real time by AFM (*38*). As gauged by these measurements, Ψ-capsids bound to the SLBs and disintegrated on them forming pore- and channel-like lesions (Fig 3A-C).

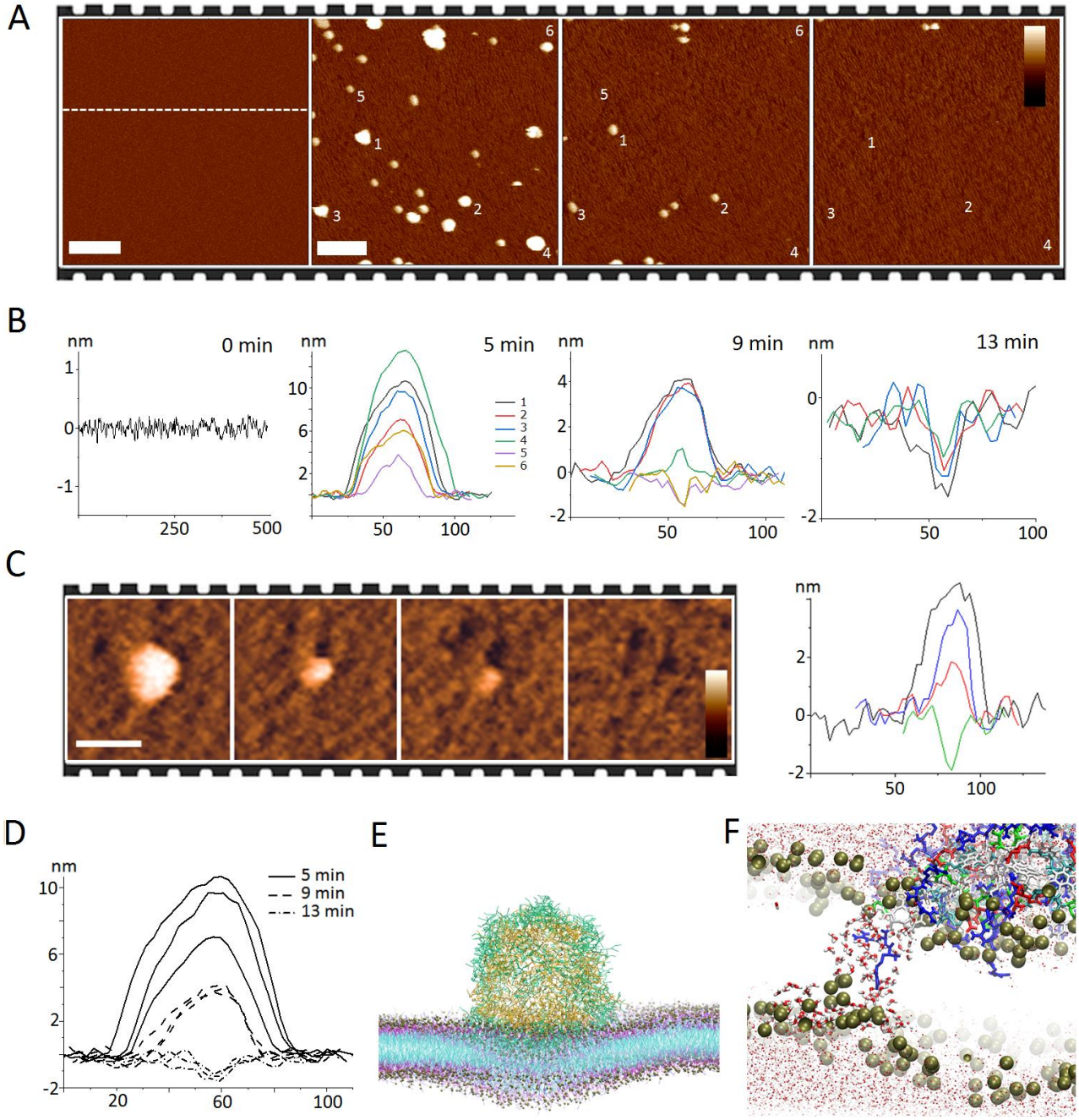

Figure 3. Pseudo-capsids porating phospholipid bilayers. (A) In liquid AFM topography of SLBs treated with D/Ψ-capsids. The images are taken at 4-min intervals. Individual Ψ-capsids are numbered (1-6) to highlight conversions into pores. Scale bars are 100 nm for the first image and 200 nm for the others. The height (colour) bar is 10 nm. (B) Cross-sectional analyses of Ψ-capsids numbered as in (A) for each given time point. (C) Topography of a Ψ-capsid converting into a pore in 15 min, with the height profiles of the corresponding conversion area. Images are taken at 5-min intervals. Scale and height (colour) bars are 50 nm and 10 nm, respectively. (D) A plot combining height profiles of three Ψ-capsids from (A) to show conversions as a function

of time. (E) A snapshot of coarse-grain MD simulations of a Ψ-capsid landing on a phospholipid bilayer at 2 μs and simulated for additional 8 μs. Key: outer and inner shells are in green and yellow, respectively; golden beads denote phosphate groups linked to two types of polar groups (blue and magenta); aliphatic lipid tails are in cyan. (F) A 72-ns snapshot from 100-ns atomistic simulations of a rudimentary pore showing a triskelion arm stretching across the bilayer interface. Key: for clarity, only phosphate groups (golden beads) are shown for the bilayer.

The conversion of individual shells into pores at their precise landing positions was complete within a few minutes of treatment: Ψ-capsids gradually sank in the lipid bilayers at the depths of a folded triskelion arm, ~1.8 nm (0.3 nm translation per β-strand residues) (Fig 3A-D). Coarse grain simulations of the capsids in the lipid bilayers (*39*) run over 10 μs revealed that the sinking effect occurred at the expense of pressing and displacing lipids deep into the bilayer interface (Fig 3E, Movie S2). In accord with this, atomistic simulations of a rudimentary pore showed that triskelion arms oriented towards the bilayer interface (Figs 3F, S6 and Movie S3). Such localised responses are consistent with a mechanism where triskelions re-assemble in the bilayer and that forming pores do not expand and remain confined within the diameters of Ψ-capsids. This is important for three reasons. First of all, the assemblies exhibit a larger structural plasticity than crystalline materials or viruses do, which allows them to rapidly re-arrange into peptide-lipid oligomers at the sites of contact with phospholipid membranes. Secondly, these oligomers maintain the size of the resulting pores close to that of the landed capsids thereby supporting precise and site-specific membrane disruption. Thirdly, this behaviour suggests that Ψ-capsids may support differential responses in cell environments favouring attack on microbial membranes. To gain a better insight into this, the biological properties of Ψ-capsids were assessed using a range of *in vitro* and *in vivo* assays.

Biological properties of pseudo-capsids

Irrespective of chirality, Ψ-capsids were found to be antimicrobial and non-hemolytic (Table S1). The minimum inhibitory concentrations (MICs) of the capsids were comparable to those of antimicrobial

agents including conventional antibiotics (Table S1). However, the principal advantage of Ψ-capsids over antimicrobial compounds lies in their ability to exert rapid and all-out damage to a bacterial cell, which makes them equally effective against susceptible and tolerant cells. In liquid AFM experiments showed that the capsids can indeed disrupt membranes within minutes. MIC experiments cannot directly relate to the AFM results as these are optical density measurements that do not take into account changes at the cellular level. Therefore, we sought complementary evidence from three series of experiments using planktonic and sessile bacterial culture of two of the most common pathogens – *E. coli* and *S. aureus*. In the first series, the antimicrobial activity of Ψ-capsids was assessed as a measure of total cell counts following capsid treatments (*27*). Negligible cell counts were observed for cultures treated with the capsids in comparison to the samples of untreated cells in which appreciable bacterial growth was observed (Fig S7). These findings provide end-point results of treated cell populations obtained over the same timescale as MIC measurements. To elucidate the antimicrobial kinetics of Ψ-capsids within the first hours and with a single-cell resolution, the second series of experiments was conducted. In these experiments thousands of individual *E. coli* cells were screened using a high throughput microfluidic device comprising thousands of growth channels (*40*). Each channel serves as a trap for an individual cell where the cell can grow through one of its distal poles, whereas the diameter of the channel matches that of the cell thereby arresting its movement (*41*). The replicative age of this trapped, mother, cell increases by one generation at each cell division allowing to follow phenotypic cell inheritance for an infinite number of generations. Such a "mother machine" then enables the single-cell monitoring of antimicrobial kinetics *in situ* and is able to reflect the responses of different cell phenotypes to antimicrobial agents (*42*). With this in mind, Ψ-capsids were introduced into *E. coli* cells trapped in the channels of the device (Fig 4A). After three hours of treatment under a constant flow the microfluidic environment was replaced by flowing the culture medium over 21 hours to restore normal conditions for bacterial growth. Subsequent analyses revealed

that Ψ-capsids killed all encountered cells (Fig 4). By contrast, persister cells and viable but not-culturable (VBNC) cells were found after ampicillin treatments (Fig 4A, B).

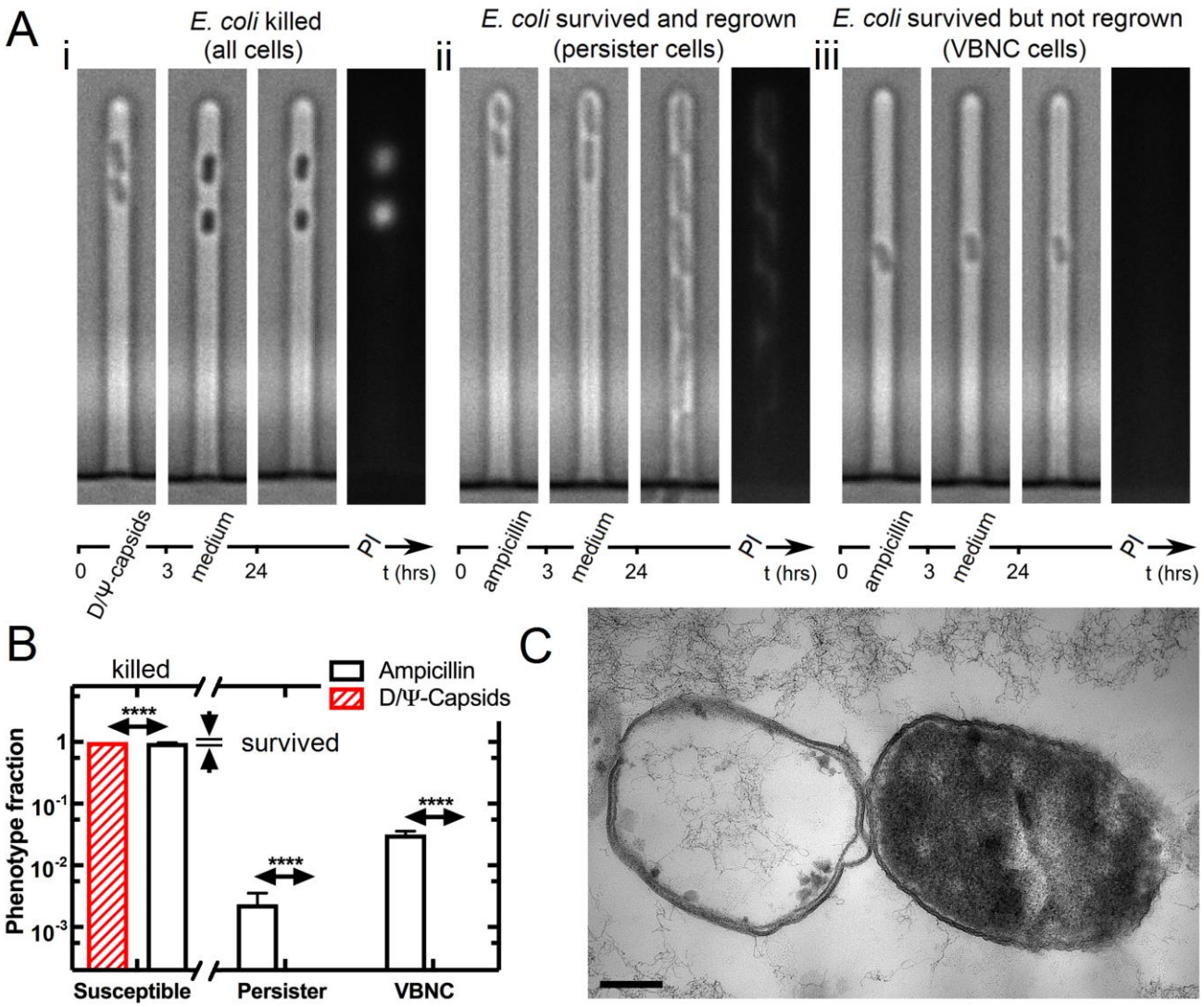

Figure 4. Single-cell antimicrobial kinetics of pseudo-capsids. (A) Three panels of representative optical micrographs of *E. coli* cells (i) killed by D/Ψ-capsids; (ii) survived and regrown after ampicillin treatments (persister cells); (iii) survived but not re-grown after ampicillin treatments (VBNC cells). In each panel, image bars show (from left to right) cells after 3-hour treatments with capsids or ampicillin, during subsequent washing with the growth medium over 21 hours, and after washing. The last micrographs in the panels are fluorescence images of 24-hour samples stained with propidium iodide (PI) – a live-dead stain penetrating dead bacteria with compromised membranes. (B) Cell fractions treated with D/Ψ-capsids and ampicillin. The data and error bars are means and standard error of the means of measurements obtained for 3332 cells hosted in 2331 independent

microfluidic channels in four independent biological replicates. The distribution of fractions of susceptible cells to ampicillin was significantly lower than that to D/Ψ-capsids (p <0.0001). The distributions of fractions of persister and VBNC cells to ampicillin were significantly higher than those to D/Ψ-capsids (p <0.0001). (C) Electron micrographs of microtomed *E. coli* cells treated with D/Ψ-capsids. The scale bar is 200 nm.

These tolerant phenotypes represent common sub-populations in clonal bacterial cultures that persist antibiotic treatments even at high doses (*43*). Persister cells resume growth after the drug is removed from their environment, whereas the regrowth of VBNC cells often requires specific conditions (*44, 45*). Both phenotypes contribute to infection relapses prompting repetitive treatments and can be linked to dormancy (*46*). With Ψ-capsids effectively reducing these phenotypes to susceptible cells, changes in cell morphology may shed light on the mechanism of action at the single cell level. Indeed, the capsid-treated cells appeared shrunk and somewhat denser when compared to unaffected cells suggesting that the capsids accumulated in the membranes. This is consistent with the AFM findings (Fig 3), though the cells in the mother machine did not disintegrate and seemed intact (Fig 4B). Therefore, cells treated with capsids were microtomed and imaged by TEM. Complete membrane destruction was evident (Figs S8). Intriguingly, however, many cells appeared as empty and half-empty carcases with displaced and bulging membranes that tended to open up at distal poles (Figs 4C, S8). This effect is not normally observed for bacteria damaged by host defence peptides or membrane-active antibiotics, which porate bacterial membranes indiscriminately, causing cells to shrink and leak (*37*) or, as polymyxins, aggregate with lipopolysaccharides into membrane-destabilising blebs across the whole bacterial surface (*47*). The emphasis on distal poles is reminiscent of bacteriophages that preferentially target the poles of bacterial cells (*48*). Although, like polymyxins, Ψ-capsids favor anionic lipids, morphologically they are more of phage mimetics that may be attracted to outward membrane curvature or cell poles serving as DNA mobilisation sites before cell division (*48, 49*). The third series of experiments provided further insight into this. The attack of Ψ-capsids on *E. coli* cells was monitored by structured illumination microscopy (SIM), which was custom designed to image

biomolecular and cellular processes in situ (*50-52*). The capsids rapidly adhered to the cell surfaces, with adsorption at the distal poles being also apparent (Figs 5A and S9A). Within a doubling time (20 min), the capsids proved to come into direct contact with the cells accumulating in their membranes and cytoplasm (Fig 5B, C). The affected cells then underwent sharp rupture accompanied by a burst of fluorescence intensity (Figs 5C, S9A-C and Movie S4). This effect was more profound in cocci cells (*S. aureus*). Although the distal poles of these cells are less defined, the transition from the initial contact with Ψ-capsids to the disintegration of their only membrane was somewhat sharper when compared to that for *E. coli* (Figs 5C, S9B and Movie S5).

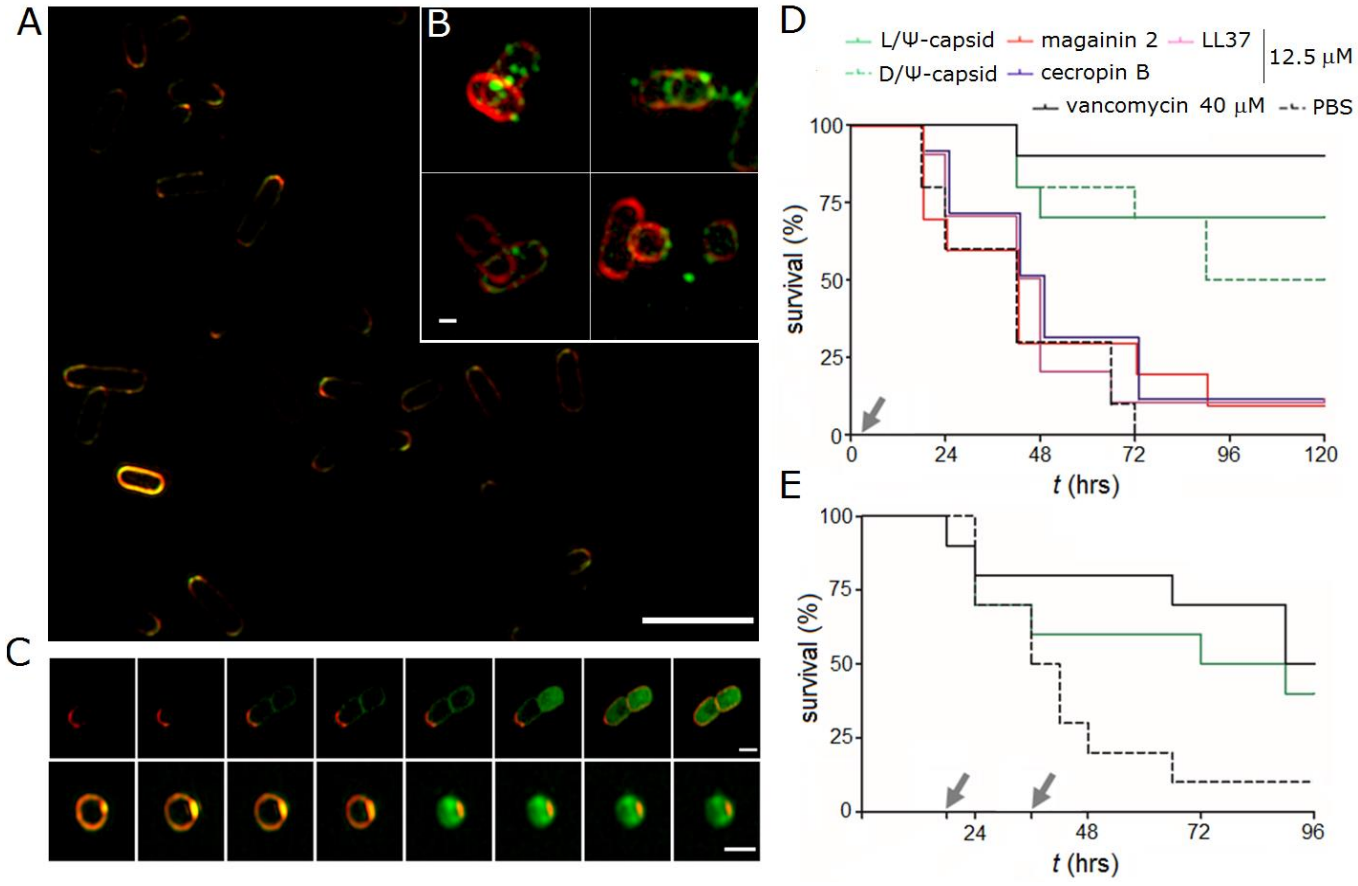

Figure 5. Time-kill kinetics of pseudo-capsids. Structured illumination micrographs of *E. coli* cells (A) immediately after the addition of L/Ψ-capsids and (B) during the treatment highlighting individual capsids in contact with cells. The capsids are labelled with carboxyfluorescein (green). Cell membranes are stained with FM4-64FX (red). Scale bars are 5 μm and 500 nm for (A) and (B), respectively. (C) SIM images recorded at 5-min intervals for *E. coli* (upper) and *S. aureus* (lower) incubated with the capsids. Scale bars are 1 μm. (D) Survival of *G. mellonella* larvae infected with vancomycin-susceptible MRSA NCTC12493 strain when treated

with Ψ-capsids and host defence peptides. Vancomycin and phosphate buffered saline (PBS) were used as positive and negative controls, respectively. Inoculations were done straight after the initiation of infection (first 2 hrs) without subsequent treatments. (E) Survival of MRSA-infected *G. mellonella* larvae treated with vancomycin, L/Ψ-capsids and PBS, administered at 18 and 36 hrs after the initiation of infection. Survival rates for Ψ-capsids were significantly higher when compared to PBS control (Mantel-Cox test, $p < 0.001$). Grey arrows indicate inoculation time points.

Strikingly, the time of cell disruption closely matched that needed for the conversion of the capsids into membrane-disrupting pores as gauged by AFM (Fig 3). Collectively, these findings suggest that Ψ-capsids need not disintegrate in the membranes, which they may effectively traverse reaching the protoplasm. Such a mode of action infers that the capsids may be able to circulate over prolonged periods of time in cellular environments that are challenged by sustained and active bacterial growth. To verify this in a biologically relevant model, Ψ-capsids were administered into *G. mellonella* larvae infected with a methicillin-resistant *S. aureus* (MRSA) strain susceptible to vancomycin (*53, 54*). Over the first 48 hours the treatments were as effective as those by high doses of vancomycin (Fig 5D). The survival rate of up to 80% proved to be steady for another 24 hours for larvae treated with D/Ψ-capsids, whereas a 10% drop was observed for larvae treated with the L-form (Fig 5D). The resulting rate of 70% did not change over the total of 120 hours of treatment for L/Ψ-capsids. In comparison, for the D-form it dropped to 50% on day 4, suggesting a depletion of the capsids in the larvae. The exact reason for this is unclear, though the decrease is likely to link to that D/Ψ-capsids were more active during the first 72 hours, possibly at the expense of more capsids being engaged with bacteria (Fig 5D). The observed survival rates proved to be superior over those reported for membrane-active antibiotics and bacteriocins implying that the capsids may indeed be equally effective in killing bacterial cells from the outside and inside (*54-56*). These experiments also demonstrated the importance of pre-assembling effector monomers into capsids, which was re-emphasised by the failure of stand-alone host-defence peptides to exert sustained antimicrobial effects under the same conditions.

Specifically, the administration of human (LL37), insect (cecropin B) and animal (magainin 2) antimicrobial peptides into the infected larvae did not improve survival rates relative to those of mock injections with PBS (Fig 5D). Furthermore, the capsids maintained high rates of bacterial clearance even when administered at significantly delayed injection times: the larvae treated with capsids at 18 and 36 hours exhibited a 50% survival up to day 4 post-infection (Fig 5E), which is twice the time achieved by bacteriophage therapies (*56*). Finally, multiple injections of the capsids into uninfected larvae did not lead to appreciable cytotoxic effects (Fig S10).

DISCUSSION

The obtained results prompt several conclusions. First of all, we have demonstrated that a discrete virus-like shell assembled from moderately antimicrobial effector molecules delivers instantaneous and irreparable damage to a bacterial cell. The damage results from a direct impact that the assembly has on the cell upon contact and ensues via multiple avenues starting with the rapid conversion of the assembled shells into membrane-disrupting pores. Remarkably, pore formation is spatially confined to the landing position of a shell, which ensures the rapid and highly localized influx of high antimicrobial doses at the site of contact. Such an impact is different from that of organic or inorganic nanoparticles that are able to rupture membranes indiscriminately by a purely physical means, are unable to disintegrate and are prone to agglomeration. In contrast, the shells are cooperative ensembles of monomeric units that are capable of re-assembly in bacterial membranes and subsequent integration into the protoplasm. Thus, secondly, these ensembles yield equilibrated nanoscale systems whose construction is symmetry driven. This is a prerequisite for the structures of this type if they are to remain autonomously operational within the nanoscale size range (*24, 57, 58*). In this regard, the polygonal architecture of viral capsids proved to be a suitable framework for templating the assembly of monomeric units, which can be of virtually any chirality and topology. An efficient strategy for the design is then to re-purpose host defence effector molecules into structurally and functionally tunable bactericidal motifs that are furnished with the ability to self-assemble. Individually, such motifs may

resemble membrane-active antibiotics or host-defence peptides, but their efficacy is no longer subject to the lag phase of reaching a critical threshold concentration on bacterial surfaces. Once assembled into a geometrically locked pseudo-capsid the motifs acquire a dual capacity of pre-concentrated and stimuli responsive antimicrobial doses. Their responsiveness builds upon their structural plasticity, which allows them to accommodate changes in dynamic environments without being restricted to a particular size (*27, 59*). Subsequently, requirements for nanoscale order are looser than those for viral subunits that tune their assembly to the size of encapsidated genomes. Similar to other protein paracrystals, which often exhibit periodic nanoscale patterns (e.g. striations or rings) (*60, 61*), the designed pseudo-capsids display fine surface structure (Fig 2A-D). Although this did not feature readily recognizable patterns, the assemblies appeared to adopt a size integer while being monomorphic in shape without competing morphologies such as filaments (*62*). Combined these physicochemical properties give rise to a highly effective antimicrobial system that, unlike antibiotics, is not frustrated by antibiotic tolerant phenotypes such as persister or VBNC cells, or by superbugs, killing all. This outcome is also notable in that the design may provide a useful tool to aid in a better understanding of how different bacteria phenotypes can be distinguished and selectively targeted (*63*). A question remains as to how universal the ability of such pseudo-capsids is in overcoming different resistance mechanisms including cell surface fortifications, efflux pump blockages or peptide antagonists that block access to cell membranes (*64-67*). As it has been long postulated (*68*) and re-emphasized most recently (*69*), host defence polypeptides are evolutionarily conserved molecules, against which a widespread resistance has yet to emerge and cannot be developed easily. Resistance mechanisms against them exist but are not deemed systemic and are readily counteracted by relatively marginal alternations in peptide structure (*69, 70*). In this light, the pseudo-capsids demonstrated here may constitute a step change in the evolution of host defence effector molecules shifting the host-pathogen arms race in favor of more sustainable and adaptable antimicrobial treatments, serving an ultimate pursuit of reducing the spread of antimicrobial resistance.

REFERENCES

1. Podolsky, S. H. The evolving response to antibiotic resistance (1945-2018). *Palgrave Commun.* **4**, 124 (2018).
2. Tacconelli, E. et al. Discovery, research, and development of new antibiotics: the WHO priority list of antibiotic-resistant bacteria and tuberculosis. *Lancet Infect Dis*. **18**, 318-327 (2018).
3. Laxminarayan, R., Matsoso, P., Pant, S., Brower, C., Røttingen, J. A., Klugman, K. and Davies, S. Access to effective antimicrobials: a worldwide challenge. *Lancet* **387**, 168-175 (2016).
4. Coates, A., Hu, Y., Bax, R. and Page, C. The future challenges facing the development of new antimicrobial drugs. *Nat. Rev. Drug Discov*. **1**, 895-910 (2002).
5. Haney, E. F., Straus, S. K. and Hancock R. E. W. Reassessing the host defense peptide landscape. *Front. Chem*. **7**, 43 (2019).
6. Hancock, R. E. and Sahl, H.-G. Antimicrobial and host-defense peptides as new anti-infective therapeutic strategies. *Nat. Biotechnol*. **24**, 1551–1557 (2006).
7. Shai, Y. Mode of action of membrane active antimicrobial peptides. *Biopolymers* **66**, 236–248 (2002).
8. Wang, G. Human antimicrobial peptides and proteins. *Pharmaceuticals* **7**, 545-594 (2014).
9. Telang, S. Lactoferrin: a critical player in neonatal host defense. *Nutrients* **10**, 1228 (2018).
10. Hunter, H. N., Demcoe, A. R., Jenssen, H., Gutteberg, T. J. and Vogel, H. J. Human lactoferricin is partially folded in aqueous solution and is better stabilized in a membrane mimetic solvent. *Antimicrob. Agents Chemother*. **49**, 3387-3395 (2005).
11. Krauzewicz, N., Stokrová, J., Jenkins, C., Elliott, M., Higgins, C. F. and Griffin, B. E. Virus-like gene transfer into cells mediated by polyoma virus pseudocapsids. *Gene Ther*. **7**, 2122-2131 (2000).

12. Saugar, I., Luque, D., Oña, A., Rodríguez, J. F., Carrascosa, J. L., Trus, B. L. and Castón, J. R. Structural polymorphism of the major capsid protein of a double-stranded RNA virus: an amphipathic alpha helix as a molecular switch. *Structure* **13**, 1007-1017 (2005).
13. Bajaj, S. and Banerjee, M. In vitro assembly of polymorphic virus-like particles from the capsid protein of a nodavirus. *Virology* **496**, 106-115 (2016).
14. Uppalapati, M. et al. A potent D-protein antagonist of VEGF-A is nonimmunogenic, metabolically stable, and longer-circulating *in vivo*. *ACS Chem. Biol*. **11**, 1058-1065 (2016).
15. Arranz-Gibert, P., Ciudad, S., Seco, J., Garcia, J., Giralt, E. & Teixido, M. Immunosilencing peptides by stereochemical inversion and sequence reversal: retro-D-peptides. *Sci. Rep*. **8**, 6446 (2018).
16. Ryadnov, M. G., Degtyareva, O. V., Kashparov, I. A. and Mitin, Y. V. A new synthetic all-D-peptide with high bacterial and low mammalian cytotoxicity. *Peptides* **23**, 1869-1871 (2002).
17. King, T. P., Wade, D., Coscia, M. R., Mitchell, S., Kochoumian, L. and Merrifield, B. Structure-immunogenicity relationship of melittin, its transposed analogues, and D-melittin. *J. Immunol*. **153**, 1124-1131 (1994).
18. Bland, J. M., De Lucca, A. J., Jacks, T. J. and Vigo, C. B. All-D-cecropin B: synthesis, conformation, lipopolysaccharide binding, and antibacterial activity. *Mol. Cell Biochem*. **218**, 105-111 (2001).
19. García-Montoya, I. A., Cendón, T. S., Arévalo-Gallegos, S. and Rascón-Cruz, Q. Lactoferrin a multiple bioactive protein: an overview. *Biochim. Biophys. Acta* **1820**, 226-236 (2012).
20. Zhao, X. Y. and Hutchens, T. W. Proposed mechanisms for the involvement of lactoferrin in the hydrolysis of nucleic acids. *Adv. Exp. Med. Biol*. **357**, 271-278 (1994).
21. Sallmann, F. R., Baveye-Descamps, S., Pattus F., Salmon, V., Branza, N., Spik, G. and Legrand, D. Porins OmpC and PhoE of *Escherichia coli* as specific cell-surface targets of human

lactoferrin. Binding characteristics and biological effects. *J. Biol. Chem*. **274**, 16107-16114 (1999).

22. Schibli, D. J., Hwang, P. M. and Vogel, H. J. The structure of the antimicrobial active center of lactoferricin B bound to sodium dodecyl sulfate micelles. *FEBS Lett*. **446**, 213-217 (1999).
23. Cochran, A. G., Skelton, N. J. and Starovasnik, M. A. Tryptophan zippers: stable, monomeric beta-hairpins. *Proc. Natl. Acad. Sci. USA*. **98**, 5578-5583 (2001).
24. Venkataram Prasad, B. V. and Schmid M. F. Principles of virus structural organization. *Adv. Exp. Med. Biol*. **726**, 17-47 (2012).
25. Kirchhausen, T. Clathrin. *Annu. Rev. Biochem*. **69**, 699-727 (2000).
26. Matsuura K. Synthetic approaches to construct viral capsid-like spherical nanomaterials. *Chem. Commun. (Camb)* **54**, 8944-8959 (2018).
27. Castelletto, V. et al. Structurally plastic peptide capsules for synthetic antimicrobial viruses. *Chem. Sci*. **7**, 1707–1711 (2016).
28. Fletcher, J. M. et al. Self-assembling cages from coiled-coil peptide modules. *Science* **340**, 595–599 (2013).
29. Mannige R. V. and Brooks C. L. 3rd. Periodic table of virus capsids: implications for natural selection and design. *PLoS One* **5**, e9423 (2010).
30. Schein, S. and Gayed, J. M. Fourth class of convex equilateral polyhedron with polyhedral symmetry related to fullerenes and viruses. *Proc. Natl. Acad. Sci. USA* **111**, 2920-2925 (2014).
31. Holowka, E. P., Sun, V. Z., Kamei, D. T. and Deming, T. J. Polyarginine segments in block copolypeptides drive both vesicular assembly and intracellular delivery. *Nat. Mater*. **6**, 52-57 (2007).
32. Oostenbrink, C., Villa, A., Mark, A. and Van Gunsteren, W. A biomolecular force field based on the free enthalpy of hydration and solvation: The GROMOS force-field parameter sets 53A5 and 53A6, *J. Comput. Chem.* **25**, 1656–1676 (2004).

33. Monticelli, L., Kandasamy, S. K., Periole, X., Larson, R. G., Tieleman, D. P. and Marrink, S. J. The MARTINI Coarse-Grained Force Field: Extension to Proteins, *J. Chem. Theory Comput.* **4**, 819–834 (2008).

34. Glasgow, J. and Tullman-Ercek, D. Production and applications of engineered viral capsids. *Appl. Microbiol. Biotechnol*. **98**, 5847–5858 (2014).

35. Maassen, S. J., van der Ham, A. M. and Cornelissen, J. L. M. Combining protein cages and polymers: from understanding self-assembly to functional materials. *ACS Macro Lett*. **5**, 987-994 (2016).

36. Noble, J. E. et al. A de novo virus-like topology for synthetic virions. *J. Am. Chem. Soc.*, **138**, 12202–12210 (2016).

37. Rakowska, P. D. et al. Nanoscale imaging reveals laterally expanding antimicrobial pores in lipid bilayers. *Proc. Natl. Acad. Sci. USA*, **110**, 8918–8923 (2013).

38. Pyne, A. et al. Engineering monolayer poration for rapid exfoliation of microbial membranes. *Chem. Sci*. **8**, 1105–1115 (2017).

39. Martínez, L., Andrade, R., Birgin, E. G. and Martínez, J. M. Packmol: a package for building initial configurations for molecular dynamics simulations. *J. Comput. Chem.* **30,** 2157-2164 (2009).

40. Wang, P., Robert, L., Pelletier, J. Dang, W. L., Taddei, F., Wright, A. and Jun, S. Robust growth of Escherichia coli. *Curr. Biol*. **20**, 1099-1103 (2010).

41. Pagliara, S., Chimerel, C., Langford, R., Aarts, D. G. and Keyser, U. F. Parallel sub-micrometre channels with different dimensions for laser scattering detection. *Lab Chip* **11**, 3365–3368 (2011).

42. Bamford, R. A., Smith, A., Metz, J., Glover, G., Titball, R. W. and Pagliara, S. Investigating the physiology of viable but non-culturable bacteria by microfluidics and time-lapse microscopy. *BMC Biol*. **15**, 121 (2017).

43. Balaban, N. Q. et al. Definitions and guidelines for research on antibiotic persistence. *Nat. Rev. Microbiol*. doi: 10.1038/s41579-019-0196-3 (2019)

44. Zhang, Y. Persisters, persistent infections and the Yin-Yang model. *Emerg. Microbes Infect.* **3**, e3 (2014).

45. Ayrapetyan, M., Williams, T. C. and Oliver, J. D. Bridging the gap between viable but non-culturable and antibiotic persistent bacteria. *Trends Microbiol*. **23**, 7–13 (2015).

46. Stapels, D. A. C., Hill, P. W. S, Westermann, A. J., Fisher, R. A., Thurston, T. L., Saliba, A. E., Blommestein, I., Vogel, J. and Helaine, S. *Salmonella* persisters undermine host immune defenses during antibiotic treatment. *Science* **362**, 1156-1160 (2018).

47. Schindler, P. R., and Teuber, M. Action of polymyxin B on bacterial membranes: morphological changes in the cytoplasm and in the outer membrane of *Salmonella typhimurium* and *Escherichia coli* B. *Antimicrob. Agents Chemother*. **8**, 95-104 (1975).

48. Edgar, R., Rokney, A., Feeney, M., Semsey, S., Kessel, M., Goldberg, M. B., Adhya, S. and Oppenheim, A. B. Bacteriophage infection is targeted to cellular poles. *Mol. Microbiol*. **68**, 1107-1116 (2008).

49. Hu, B., Margolin, W., Molineux, I. J. and Liu, J. Structural remodeling of bacteriophage T4 and host membranes during infection initiation. *Proc. Natl. Acad. Sci. USA* **112**, E4919-E4928 (2015).

50. Shaw, M., Zajiczek, L. and O'Holleran, K. High Speed Structured Illumination Microscopy in Optically Thick Samples. *Methods* **88**, 11−19 (2015).

51. O'Holleran, K. and Shaw, M. Optimized approaches for optical sectioning and resolution enhancement in 2D structured illumination Microscopy. *Biomed. Opt. Express* **5**, 2580−2590 (2014).

52. Shaw, M., Bella, A. and Ryadnov, M. G. CREIM: Coffee ring effect imaging model for monitoring protein self-assembly in situ. *J. Phys. Chem. Lett*. **8**, 4846-4851 (2017).

53. Desbois, A. P. and Coote, P. J. Wax moth larva (*Galleria mellonella*): an in vivo model for assessing the efficacy of antistaphylococcal agents. *J. Antimicrob Chemother,* **66**, 1785-1790, (2011).

54. Ba, X. *et al.* Old drugs to treat resistant bugs: methicillin-resistant *Staphylococcus aureus* isolates with mecC are susceptible to a combination of penicillin and clavulanic acid. *Antimicrob. Agents Chemother.* **59**, 7396-7404, (2015).

55. Gibreel, T. M. and Upton, M. Synthetic epidermicin NI01 can protect *Galleria mellonella* larvae from infection with *Staphylococcus aureus*. *J. Antimicrob. Chemother*. **68**, 2269-2273 (2018).

56. Takemura-Uchiyama, I., Uchiyama, J., Kato, S., Inoue, T., Ujihara, T., Ohara, N., Daibata, M. and Matsuzaki, S. Evaluating efficacy of bacteriophage therapy against *Staphylococcus aureus* infections using a silkworm larval infection model. *FEMS Microbiol. Lett*. **347**, 52-60 (2013).

57. De Santis, E, et al. Antimicrobial peptide capsids of de novo design. *Nat Commun*. **8**, 2263 (2017)

58. Matsuura, K. Construction of spherical virus-inspired peptide nanoassemblies. *Polym. J.* **44**, 469–474 (2012).

59. Tarasov, S. G. et al. Structural plasticity of a transmembrane peptide allows self-assembly into biologically active nanoparticles. *Proc. Natl. Acad. Sci. USA* **108**, 9798–9803 (2011).

60. Ryadnov, M. G. A self-assembling peptide polynanoreactor. *Angew. Chem. Int. Ed*. **46**, 969–972 (2007).

61. Papapostolou, D., Smith, A. M., Atkins, E. D., Oliver, S. J., Ryadnov, M. G., Serpell, L. C. and Woolfson, D. N. Engineering nanoscale order into a designed fiber. *Proc. Natl. Acad. Sci USA* **104**, 10853-10858 (2007).

62. Matsuura, K., Murasato, K. and Kimizuka, N. Artificial peptide nanospheres self-assembled from three-way junctions of β-sheet-forming peptides. *J. Am. Chem. Soc.* **127**, 10148–10149 (2005).

63. Brauner, A., Fridman, O., Gefen, O. and Balaban, N. Q. Distinguishing between resistance, tolerance and persistence to antibiotic treatment. *Nat. Rev. Microbiol*. **14**, 320-330 (2016).

64. Neuhaus, F. C. and Baddiley, J. A continuum of charge: structures and functions of D-alanyl-teichoic acids in Gram-positive bacteria. *Microbiol. Mol. Biol. Rev.* **67**, 686–723 (2003).

65. Needham, B. D. and Trent, M. S. Fortifying the barrier: the impact of lipid A remodeling on bacterial pathogenesis. *Nat. Rev. Microbiol.* **11**, 467–481 (2013).

66. Joo, H.-S., Fu, C.-I. and Otto, M. Bacterial strategies of resistance to antimicrobial peptides. *Phil. Trans. R. Soc. B* **371**, 20150292 (2016).

67. Ryan, L. *et al*. Anti-antimicrobial peptides: folding-mediated host defense antagonists. *J. Biol. Chem.* **288**, 20162–20172 (2013).

68. Zasloff, M. Antimicrobial peptides of multicellular organisms. *Nature* **415**, 389–395 (2002).

69. Lazar, V. et al. Antibiotic-resistant bacteria show widespread collateral sensitivity to antimicrobial peptides *Nat. Microbiol*. **3**, 718-731 (2018).

70. Pfeil, M. P. et al. Tuneable poration: host defense peptides as sequence probes for antimicrobial mechanisms. *Sci. Rep*. **8**, 14926 (2018).

Supplementary information contains experimental notes together with additional data, table and figures

Acknowledgements

We acknowledge funding from the UK's Department for Business, Energy and Industrial Strategy. UL and SP were supported through an MRC Proximity to Discovery EXCITEME2 grant (MCPC17189).

Author contributions

All authors designed and performed the experiments. M.G.R wrote the manuscript. All authors analysed data and contributed to the editing of the manuscript.

Additional Information

The authors declare no competing financial interests. Correspondence and requests for materials should be addressed to M.G.R.